ISBN: 978-3-95450-223-3 ISSN: 2673-7000 doi:10.18429/JACoW-NAPAC2019-MOPLH24

TOWARDS THE OPTIMIZATION OF PHOTOCATHODE PROPERTIES VIA SURFACE SCIENCE TECHNIQUES: A STUDY ON Cs_3Sb THIN FILM GROWTH*

A. Galdi †, J. Balajka, J. B. Baretz, I. V. Bazarov, L. Cultrera, W. J. I. DeBenedetti, M. A. Hines, F. Ikponwmen, J. M. Maxson, S. A. McBride
Cornell University, Ithaca NY, USA

Abstract

Surface science measurement techniques such as x-ray photoemission spectroscopy (XPS) and scanning tunnel microscopy (STM) can provide quantitative information about the composition and the morphology of thin film samples. We successfully transferred Cs-Sb samples from the growth chamber to a surface science XPS/STM system by use of an UHV suitcase and measured their properties. This will allow to study the properties of photocathode films and ultimately how to control the growth process to achieve the best performances, including high efficiency, ruggedness and low emittance.

INTRODUCTION

Photocathodes are the electron sources of choice for cutting edge linear accelerator applications, such as free electron lasers (FEL) [1] and ultrafast electron diffraction (UED). [2] The transverse momentum spread of the photoemitted electrons is critical for these applications, since it determines the shortest achievable wavelength in FEL and the coherence lenght for electron diffraction. When high efficiency is required, alkali antimonide based photocathodes have demonstrated to have excellent performance with visible light. [3] At the same time, when operated at cryogenic temperatures (90 K) and near the photoemission threshold (690 nm), they provide electron beams characterized by very low intrinsic emittance, down to 0.17 μm/mm (i.e. the normalized emittance per unit area, proportional to the rms transverse momentum). [4] A limiting factor to achieving the lowest possible intrinsic emittance has been identified in the surface inhomogeinities of photocathodes, such as the surface roughness and workfunction variations. [5, 6] The study of the surface properties of this class of materials is limited by their reactivity, that require the samples to be in ultra-high vacuum (UHV) to avoid degradation and decomposition. X-ray photoemission spectroscopy (XPS) has been a powerful tool to characterize the composition and reactivity of alkali antimonides, thanks to its particular sensitivity to the surface composition. [7–11] Scanning probe techniques, such as atomic force microscopy in UHV, have been employed to characterize the morphology and roughness. [12] Another very powerful technique is scanning tunnel microscopy (STM), that is typically performed in UHV and it is capable to achieve atomic-scale resolution. UHV suitcases are typically used to transport air-sensitive cathodes from the growth system to the photoinjector. [11, 13] Here we use a vacuum suitcase to interface the alkali antimonide growth system to a standard XPS-STM surface science apparatus, using commercially available sample holders and manipulation tools. The first results on coupled STM and XPS measurements on Cs-Sb thin film samples grown on different substrates are presented.

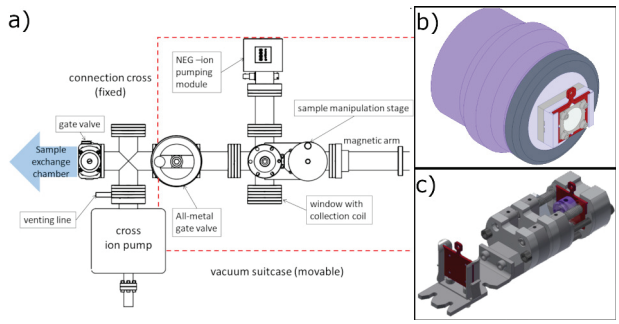

Figure 1: (a) schematics of the vacuum suitcase; (b) standard growth puck (purple) with the adapter (light purple) holding the Omicron sample holder (red). The sample (light yellow) is held by a metal retaining plate and screws (light gray); (c) multi sample carrier installed in the vacuum suitcase.

EXPERIMENTAL

Film Growth and Transfer

Cs-Sb samples were deposited on (001) rutile TiO_2 and (10-10) Al_2O_3 insulating substrates. Lattice-matched substrates are of interest to promote anisotropic growth of Cs_3Sb and possibly yielding single oriented, lower roughness surfaces.

The Cs-Sb samples were grown in the growth system described in ref. [14] at a temperature of 70°C , using pure Cs and Sb metals. Substrates were mounted on an standard sample holder shown in Fig.1(b), using a metal retaining plate in order to provide electrical contact to the sample surface (relevant both to measure the photocurrent during growth and for successive STM-XPS measurements); the sample plate was then installed on the standard growth puck. [14] The photocurrent emitted by the sample was monitored during growth by exciting the cathode with a 504 nm diode laser and by measuring the drain current from the cathode biased at -18 V with a lock-in amplifier locked to the fre-

* This work was supported by the U.S. National Science Foundation under Awards OIA-1549132, the Center for Bright Beams, and PHYS-1535279.
† ag733@cornell.edu

ISBN: 978-3-95450-223-3 ISSN: 2673-7000 doi:10.18429/JACoW-NAPAC2019-MOPLH24

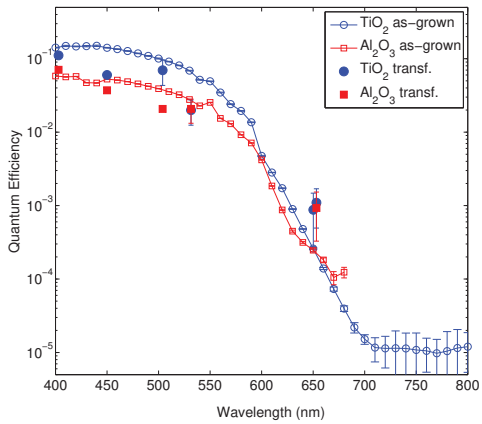

Figure 2: Spectral response of the sample grown on Al_2O_3 (red) and TiO_2 (blue). Open symbols represent the data collected after growth in-situ and filled symbols the measurements performed after the transfer to the STM-XPS analysis system.

quency of an optical chopper that modulates the incident laser beam. Typical fluxes were 10^{13} atoms/cm^2/s for Cs and 3×10^{12} atoms/cm^2/s for Sb; the fluxes were fine adjusted by monitoring the photocurrent. Cs and Sb were codeposited until a Sb equivalent thickness of about 10-15 nm is reached, that, in the hypothesis that stoichiometric Cs_3Sb is formed, corresponds to a total thickness of 60-100 nm. [15] After the growth, the samples were transferred to an exchange chamber (P=1×10^{-10} Torr), where the Omicron sample plate is extracted from the growth puck and loaded in the UHV vacuum suitcase shown in Fig. 1(a), capable of maintaining pressure of the order of 10^{-10} Torr, as measured by the ion pump current. Once the samples were loaded in the vacuum suitcase, the all metal gate valve was closed and the connection cross vented to disconnect the suitcase. The suitcase was then connected to the load-lock chamber of the analysis system. The load-lock was previously baked until the vacuum reached $\approx 10^{-10}$ Torr; the load-lock was then vented with pure N_2 gas and connected to the suitcase and pumped until attaining a pressure of about 2.5×10^{-10} Torr before opening the gate valve for the sample transfer.

XPS and STM Measurements

XPS measurements were performed using a Mg $K\alpha$ source. The angle between the sample surface normal and the electron analyzer aperture (take-off angle) was varied from 0° and 70°. Due to the angular dependence of the escape depth of photoelectrons (that is of the order of few nm), the grazing take-off measurements are more sensitive to the sample surface, since they probe a smaller thickness. STM measurements were performed at room temperature using using a W tip and an Omicron variable-temperature STM.

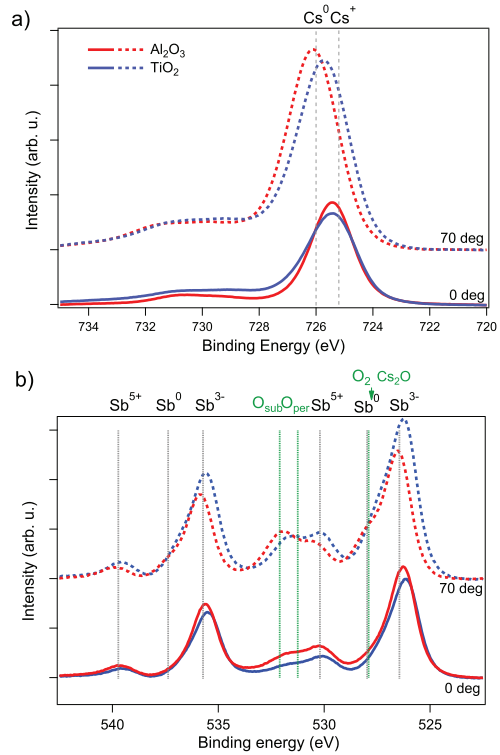

Figure 3: XPS spectra of the sample grown on Al_2O_3 and on TiO_2 substrates measured at 0° (solid lines) and 70° take off angle, (a) at the Cs $3d^{5/2}$ and (b) at the Sb $3d^{3/2}$–$3d^{5/2}$ edges. In (b) the energies corresponding to various Sb valences and oxygen species (O_{sub}: Cs suboxide, O_{per}: O_2^{2-} in Cs_2O_2) are reported by gray and green dashed lines respectively.

RESULTS AND DISCUSSION

The spectral response of the Cs-Sb thin films was measured after the growth, in a chamber connected to the growth one, by using a lamp and a monochromator, and by measuring the drain current of the sample biased at -18 V. The measurement was repeated after the transfer in the analysis chamber, by using a set of laser diodes and collecting the photocurrent via a coil biased at 200 V. The results are reported in Figure 2; the quantum efficiency after the transfer is very close to the initial one. In Figure 3 we report the XPS measurements of the two samples for different take-off angles at the Cs and Sb binding energies. The less surface sensitive 0° measurements are very similar for the two samples, while some differences are evident in the 70° spectra. The Cs peak, in Figure 3 (a), shifts from a binding energy close to the one of Cs^+ (as in Cs_3Sb) towards the energy of metallic Cs, in particular for the Al_2O_3 substrate. The Sb $3d$ edge, reported Figure 3 (b), occurs in the same energy range of the O $1s$ one ([527,533] eV), hence the spectra contain information from both species. Oxygen can be present in Cs-Sb samples due to residual gas (O_2 or H_2O) in the growth and storage chambers [9, 10, 16], or to contamination during the transfer process. The $3d^{3/2}$ ([532, 542] eV) and $3d^{5/2}$ ([532, 520] eV) peaks are related by spin-orbit splitting: the

ISBN: 978-3-95450-223-3 ISSN: 2673-7000 doi:10.18429/JACoW-NAPAC2019-MOPLH24

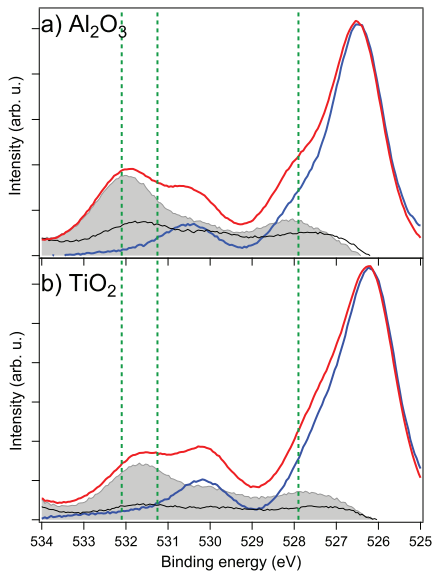

Figure 4: Sb $3d^{5/2}$ XPS spectrum of (a) the Al_2O_3 substrate sample and (b) the TiO_2 one. Red lines represent the 70° take-off angle Sb $3d^{5/2}$ peak, blue lines the Sb $3d^{3/2}$ peak translated by the spin-orbit splitting energy and multiplied by 1.5. The grey shadowed area is the difference spectrum, the black line is the same difference for 0° take-off angle.

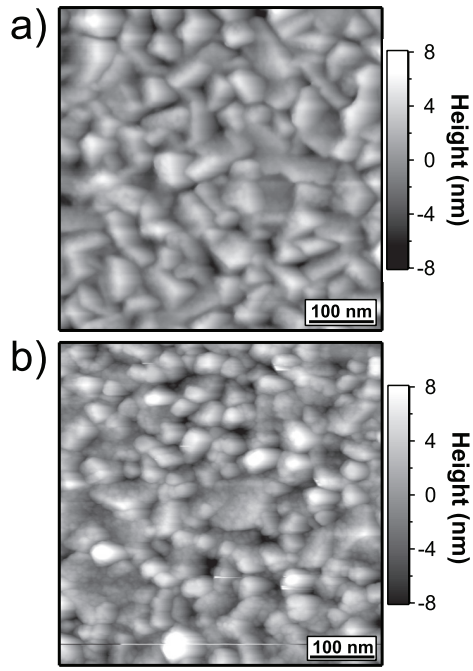

Figure 5: STM images of (a) the sample grown on Al_2O_3 and (b) the sample grown on TiO_2.

former differs from the latter for a translation of 9.4 eV and intensity ratio of 1.5. [9] From the $3d^{3/2}$ peaks we can see that the majority of Sb is in the 3- valence typical of Cs_3Sb, while some is Sb^{5+}, indicating the presence of Sb_2O_5. In the surface sensitive 70° data, a shoulder at 537.4 eV reveals the presence of metallic Sb. The oxygen contribution can be singled out by subtracting the translated and rescaled $3d^{3/2}$ peaks from the $3d^{5/2}$ region, as shown in Figure 4. The difference spectrum has a maximum at about 532.1 eV, corresponding to oxygen in Cs suboxide ($Cs_{11}O_3$); weaker contributions from Sb oxide at 530 eV and Cs_2O at 528.3 eV can also be identified. [9, 17] By comparing our results with those present in literature [7–9, 16], our results are in agreement with the formation of a predominantly Cs suboxide and elemental Sb layer on the sample surface. Additionally some Sb and Cs oxides are also formed. Light oxidation can even enhance the quantum efficiency of Cs_3Sb due to the band-bending effect of $Cs_{11}O_3$, in particular at long wavelengths.

In Figure 5 we report the STM images of the samples. Both samples show a similar morphology with structures that we can identify as grains, with a size of few 10s of nm and height variation of the order of 10 nm. The structure of the samples is very similar to previous measurements performed on samples grown on Si substrates, suggesting no particular influence of the substrate on the film growth in the present conditions. In conclusion the investigated samples have similar composition in the bulk, as revealed by the 0° take-off angle XPS spectra. The surface sensitive XPS measurements reveal a higher oxygen content on the surface of the Al_2O_3 substrate sample. Since both samples were transferred together, we cannot attribute the different oxidation of the two samples to the transfer process. However the sample grown on Al_2O_3 was grown 5 days before the sample on TiO_2, and it has possibly adsorbed a larger amount of oxygen while being stored in the storage chamber or in the vacuum suitcase. The samples appear polycrystalline with small grains (10s of nm); systematic studies are required to link the morphology to the growth condition and to the surface oxidation.

CONCLUSIONS

We successfully transferred Cs-Sb thin film samples from the growth system to a XPS-STM analysis system via UHV suitcase. The samples were grown on insulating oxide substrates with possible lattice matching with the Cs_3Sb unit cell structure. Despite the substrate being insulating, quantum efficiency, XPS and STM measurements could be performed. Our results pave the way to systematic studies on the effect of substrate materials and growth conditions on the physical properties of Cs-Sb photocathode films, with the aim of achieving epitaxial single oriented films with improved properties.

REFERENCES

[1] P. e. a. Emma, "First lasing and operation of an angstrom wavelength," *Nature Photonics*, 2010.

[2] A. H. Zewail, "4d ultrafast electron diffraction, crystallography, and microscopy," *Annual Review of Physical Chemistry*, vol. 57, no. 1, pp. 65–103, 2006. PMID: 16599805.

ISBN: 978-3-95450-223-3 ISSN: 2673-7000 doi:10.18429/JACoW-NAPAC2019-MOPLH24

[3] L. Cultrera, S. Karkare, B. Lillard, A. Bartnik, I. Bazarov, B. Dunham, W. Schaff, and K. Smolenski, "Growth and characterization of rugged sodium potassium antimonide photocathodes for high brilliance photoinjector," *Applied Physics Letters*, vol. 103, no. 10, p. 103504, 2013.

[4] L. Cultrera, S. Karkare, H. Lee, X. Liu, I. Bazarov, and B. Dunham, "Cold electron beams from cryocooled, alkali antimonide photocathodes," *Physical Review Special Topics - Accelerators and Beams*, vol. 18, no. 11, p. 113401, 2015.

[5] S. Karkare and I. Bazarov, "Effect of nanoscale surface roughness on transverse energy spread from gaas photocathodes," *Applied Physics Letters*, vol. 98, no. 9, p. 094104, 2011.

[6] G. Gevorkyan, S. Karkare, S. Emamian, I. V. Bazarov, and H. A. Padmore, "Effects of physical and chemical surface roughness on the brightness of electron beams from photocathodes," *Phys. Rev. Accel. Beams*, vol. 21, p. 093401, Sep 2018.

[7] C. W. Bates, D. D. Gupta, L. Galan, and D. Buchanan, "X-ray photoemission studies of cesium antimonide photoemitters," *Thin Solid Films*, vol. 69, no. 2, pp. 175 – 182, 1980.

[8] C. W. Bates, T. M. van Atekum, G. K. Wertheim, D. N. E. Buchanan, and K. E. Clements, "Xray photoemission studies of superficially oxidized cesium antimonide photoemitters," *Applied Physics Letters*, vol. 38, no. 5, pp. 387–389, 1981.

[9] L. Soriano and L. Galán, "Interaction of Cesium-Potassium Antimonide Photocathode Materials with Oxygen: an X-Ray Photoelectron Spectroscopy Study," *Japanese Journal of Applied Physics*, vol. 32, pp. 4737–4744, oct 1993.

[10] I. Martini, E. Chevallay, V. Fedosseev, C. Hessler, H. Neupert, V. Nistor, and M. Taborelli, "X-ray Photoemission Spectroscopy Studies of Cesium Antimonide Photocathodes for Photoinjector Applications," in *Physics Procedia*, 2015.

[11] M. A. H. Schmeißer, S. Mistry, H. Kirschner, S. Schubert, A. Jankowiak, T. Kamps, and J. Kühn, "Towards the operation of cs-k-sb photocathodes in superconducting rf photoinjectors," *Phys. Rev. Accel. Beams*, vol. 21, p. 113401, Nov 2018.

[12] J. Feng, S. Karkare, J. Nasiatka, S. Schubert, J. Smedley, and H. Padmore, "Near atomically smooth alkali antimonide photocathode thin films," *Journal of Applied Physics*, vol. 121, no. 4, p. 044904, 2017.

[13] L. Cultrera, I. Bazarov, J. Convay, B. Dunham, S. Karkare, Y. Li, X. Liu, J. Maxson, and K. Smolenski, "Growth and characterization of rugged sodium potassium antimonide photocathodes for high brilliance photoinjector," *Proceedings of the 24th Particle Accelerator Conference, PAC-2011*, p. WEP244, 2011.

[14] L. Cultrera, H. Lee, and I. Bazarov, "Alkali antimonides photocathodes growth using pure metals evaporation from effusion cells," *Journal of Vacuum Science & Technology B, Nanotechnology and Microelectronics: Materials, Processing, Measurement, and Phenomena*, vol. 34, no. 1, p. 011202, 2016.

[15] J. Xie, M. Demarteau, R. Wagner, S. Schubert, M. Gaowei, K. Attenkofer, J. Walsh, J. Smedley, J. Wong, J. Feng, H. Padmore, M. Ruiz-Oses, Z. Ding, X. Liang, E. Muller, and I. Ben-Zvi, "Synchrotron x-ray study of a low roughness and high efficiency K2CsSb photocathode during film growth," *Journal of Physics D: Applied Physics*, vol. 50, no. 20, p. 205303, 2017.

[16] L. Danielson, C. Lee, and P. Oettinger, "Laser illuminated high current photocathodes," *Applications of Surface Science*, vol. 16, no. 1, pp. 257 – 267, 1983.

[17] S.-J. Yang and C. W. Bates, "The role of cesium suboxides in low-workfunction surface layers studied by x-ray photoelectron spectroscopy: Ag-o-cs," *Applied Physics Letters*, vol. 36, no. 8, pp. 675–677, 1980.